PHYSICAL REVIEW B **89**, 121412(R) (2014)

Doping-dependent band structure of $LaAlO_3/SrTiO_3$ interfaces by soft x-ray polarization-controlled resonant angle-resolved photoemission

C. Cancellieri,* M. L. Reinle-Schmitt, M. Kobayashi, V. N. Strocov, and P. R. Willmott
Swiss Light Source, Paul Scherrer Institut, CH-5232 Villigen, Switzerland

D. Fontaine and Ph. Ghosez
Physique Théorique des Matériaux, Université de Liège, Allée du 6 Août 17 (B5), 4000 Sart Tilman, Belgium

A. Filippetti, P. Delugas, and V. Fiorentini
CNR-IOM UOS Cagliari, Dipartimento di Fisica, Università di Cagliari, SP Monserrato-Sestu km.0.700, 09042 Monserrato (CA), Italy

(Received 17 July 2013; revised manuscript received 11 March 2014; published 27 March 2014)

Polarization-controlled synchrotron radiation was used to map the electronic structure of buried conducting interfaces of $LaAlO_3/SrTiO_3$ in a resonant angle-resolved photoemission experiment. A strong polarization dependence of the Fermi surface and band dispersions is demonstrated, highlighting different Ti $3d$ orbitals involved in two-dimensional (2D) conduction. Measurements on samples with different doping levels reveal different band occupancies and Fermi-surface areas. The photoemission results are directly compared with advanced first-principles calculations, carried out for different $3d$-band filling levels connected with the 2D mobile carrier concentrations obtained from transport measurements, with indication of charge localization at the interface.

DOI: 10.1103/PhysRevB.89.121412 PACS number(s): 73.20.−r, 71.15.Mb, 79.60.Jv

Complex-oxide interfaces exhibit a broad spectrum of electronic properties and complex phase diagrams and have thus attracted considerable attention. A particularly interesting example is the appearance of two-dimensional (2D) conductivity at the interface between the band insulators $LaAlO_3$ (LAO) and $SrTiO_3$ (STO) [1–3] above a critical LAO thickness of three unit cells (u.c.) [4]. *Ab initio* calculations [5,6] reveal that the mobile electron charge of this two-dimensional electron system (2DES) is confined in conduction bands of $3d$ t_{2g} orbital character extending over a few STO layers from the interface and is thus very different from that of doped bulk STO. However, the detailed characteristics of these conduction bands crucially depend on the amount of carriers present at the interface. A comparison between observed and calculated electronic properties of the interface thus only makes sense if referred to the same carrier concentration.

The band structure calculated for 0.5 electrons per u.c. (3.3×10^{14} e/cm^2), that is, the value needed to suppress the "polar catastrophe" due to the diverging potential in polar LAO [7], is often taken as the "reference." In fact, the experimentally determined mobile carrier density in LAO/STO is always smaller. Typical experimental values reported for the 2D-sheet carrier density, n_s, measured by the Hall effect at 100 K are between 10^{13} and 10^{14} e/cm^2 [8]. This suggests an important partial charge localization or other charge-compensating mechanisms, such as surface passivation or reconstruction [9,10].

Direct access to the electronic band structure is a crucial step towards a full understanding of complex-oxide interfaces. Angle-resolved photoemission spectroscopy (ARPES) is a powerful technique which yields a map of photoelectron intensities as a function of their kinetic energies and momentum, revealing the electronic structure in solids. Recent ARPES studies on bare STO surfaces [11–13] appeared similar to those of the LAO/STO interfacial conducting layer. ARPES of buried interfaces is more challenging due to the small inelastic electron mean free path in solids, which, over a wide range of photon energies, is of the order of 1 nm. However, it was recently shown that a combination of soft x-ray ARPES with resonant photoexcitation [14–18] can overcome this limitation. By selecting the photon energy $h\nu$ at the Ti L edge, the signal of the Fermi states associated with 2D conductivity is greatly enhanced in LAO/STO interfaces. Berner and co-workers [18] were the first to report on the Fermi surface (FS) of the LAO/STO interface, confirming the similarities between bare STO and STO-based heterostructures. Here we report ARPES measurements of differently doped interfaces, measured with unsurpassed energy resolution not only as a function of angle, but also of photon polarization. In this manner, we are able to distinguish different orbital contributions to the bands and FS.

We have correlated the FS shape with the number of carriers measured by magnetotransport by investigating samples with different n_s. The FS and band dispersions are highly dependent on the incident photon light polarizations and on n_s, suggesting a strong orbital character and different band filling. The experimental data are complemented by *ab initio* calculations, which describe the detailed evolution of band energies and FS with the interfacial charge density, in a range ($\sim 10^{13}$ e/cm^2), consistent with those measured by the Hall effect for the investigated samples. This provides an unprecedented, direct comparison of calculated and measured electronic properties at the same doping. Our ARPES dispersions and theoretical calculations coherently reproduce the orbital distribution of charges at the given transport-derived carrier density, thus clarifying the exact $3d$-level electron occupancy, with remnant difference between the experiment and theory revealing presumably electron localization at the interface. The possible contribution of photocarriers induced by x radiation was investigated and only an insignificant effect on the electronic structure was measured. Details are given in the Supplemental Material [19].

*claudia.cancellieri@psi.ch

LAO thin films were grown by pulsed laser deposition on (001)-oriented TiO_2-terminated STO substrates at 800 °C in an oxygen pressure of 8×10^{-5} mbar. A KrF excimer laser (248 nm) was used to ablate the sintered targets with a fluence of 0.6 J/cm^2 at a frequency of 1 Hz, leading to a deposition rate of one unit cell for ~ 60 pulses. After deposition, the O_2 pressure was raised to 0.2 bar and the temperature was held at 540 ± 10 °C for one hour, in order to ensure full oxidation [20]. Film growth was monitored *in situ* by reflection high-energy electron diffraction. "Standard" LAO/STO samples have transport properties similar to those reported in Ref. [8], with $n_s \sim 4$–6×10^{13} e/cm^2, measured by the Hall effect (SD samples). Samples with lower 2D-carrier densities (LD samples) were also prepared using a growth temperature of 650 °C, as reported in Ref. [21]. These samples have $n_s \sim 10^{13}$ e/cm^2. Our conducting interfaces had a LAO thickness slightly larger than 4 u.c. to ensure full conductivity. For each of the two doping levels, at least three samples were grown and measured in order to confirm the reproducibility of the presented results.

An advanced variant of density functional theory was used: the variational pseudo-self-interaction correction (VPSIC) [22]. This is capable of correcting the imperfect description of standard local-density functionals and reproduces the band gap of oxide-based systems and the band alignment at the LAO/STO interface [6]. The different carrier-density regimes are described, starting from the insulating interface (i.e., for LAO thickness smaller than 4 u.c.) and, while keeping the LAO thickness fixed, introducing an increased amount of electron charge in the system, Q, and leaving the system to fully relax to its structural and electronic ground state (in practice, mimicking a field-effect-induced charge accumulation). In this way, the evolution of the electronic properties due to tiny but well-defined changes of electron charge, comparable in magnitude with the Hall-measured values, can be monitored. The band dispersion in the 2DES system was calculated by VPSIC for the charge densities $Q = 0.04$ and 0.1 e/u.c., matching the experimental n_s values of 2.6×10^{13} e/cm^2 and 6.5×10^{13} e/cm^2 for the LD and SD samples, respectively. The results are shown in Figs. 1(a) and 1(b) (other Q values are presented in the Supplemental Material [19]). The 2D FSs corresponding to the shown bands are illustrated in Figs. 1(c) and 1(d) (for details of the band evolution as a function of Q, see the Supplemental Material [19]). Not only does the surface break the degeneracy of the d_{xy} and $d_{yz,xz}$ states, but also the quantum well near the surface created by the varying potential splits each of them into separate bands [21]. First, our calculations show that while the in-plane effective masses of the t_{2g} bands are scarcely affected by the interface, importantly, their band bottom alignment with respect to the Fermi energy E_F, as well as their mutual band splitting, depend crucially on the overall amount of mobile charge Q in the system. At very low density, mobile charge accumulates in the d_{xy} bands closer to the interface (red and green dots), while orthogonal d_{yz} and d_{xz} orbitals (blue dots) are initially empty. Such a d_{xy}-(d_{yz},d_{xz}) on-site splitting is a well-known consequence of the conduction-band misalignment and suppression of interface orthogonal hopping. As the pocket area and Fermi vector k_F increase progressively with the carrier density, for $n_s \geqslant 3 \times 10^{13}$ e/cm^2 ($Q \geqslant 0.04$) the orthogonal cigar-shaped orbitals begin to emerge. Given the different character of the planar and orthogonal orbitals, crossing this threshold represents a dramatic change in the optical and transport properties of the 2DES.

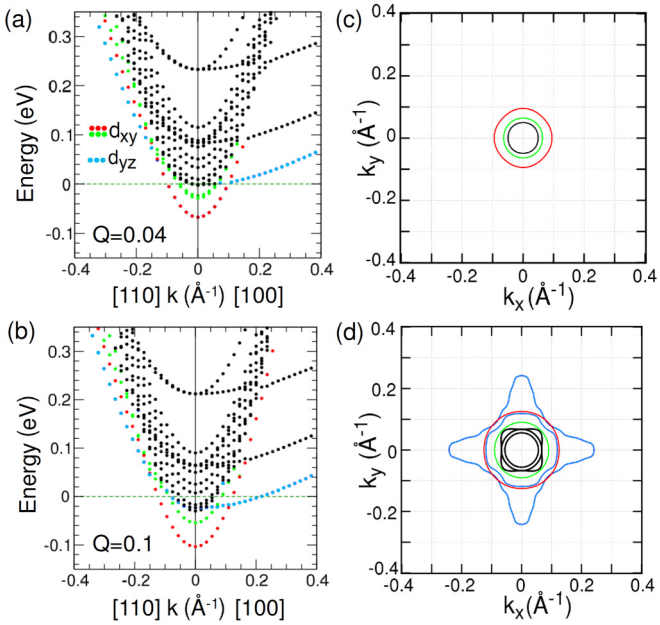

FIG. 1. (Color online) Band energies of LAO/STO calculated at (a) $Q = 0.04$ and (b) $Q = 0.1$. The most populated bands are highlighted in color, indicating their character. The corresponding FSs are shown in (c) and (d).

ARPES measurements were performed at the soft x-ray ARPES end station of the Advanced Resonant Spectroscopies (ADRESS) beam line [23] at the Swiss Light Source. The samples were transferred from the deposition chamber *ex situ* without further annealing in vacuum. The beam line delivers a high photon flux, exceeding 10^{13} photons/sec/0.01% bandwidth, providing excellent statistics of the photoelectron signal, despite its attenuation as it passes through the film layer. Measurements were performed using *c*-polarized (circular), *p*-polarized (linear vertical), and *s*-polarized (linear horizontal) radiation to excite states of different symmetry relative to the mirror plane. The measurement plane (MP) coincides with the (010) mirror plane defined by the sample normal along the [001] and the Γ-*X* directions [Fig. 2(a)]. The experiment was performed at ∼11 K. The combined beam line and analyzer energy resolution was set to around 80 meV for the valence-band spectra.

Following Ref. [17], $h\nu = 460.3$ eV was selected at the Ti *L* absorption edge (see Supplemental Material [19]). Importantly, no in-gap states could be detected in the samples at any photon energy (see also Supplemental Material [19] for results on the related $La_{0.5}Sr_{0.5}Al_{0.5}Ti_{0.5}O_3$/STO heterostructure [24]). These in-gap states, measured in bare STO [11,13,25] and very recently also in the LAO/STO interface [18,26], appear at ≈ 1 eV below E_F, are resonant with Ti^{3+} valence states, and are possibly due to surface defects and impurity states related to oxygen vacancies [27]. These incoherent states are highly photosensitive, exhibiting a pronounced photodoping effect. Our oxygen-annealed samples show no such contributions, which is also confirmed by negligible

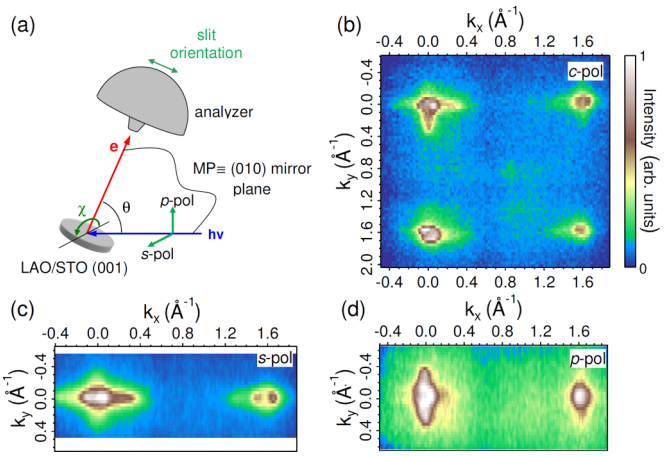

FIG. 2. (Color online) (a) Experimental geometry for polarization-dependent measurements: χ and θ allow in-plane k-space mapping. ARPES data for the SD samples: (b) FS maps collected for four Brillouin zones with c-polarized light at 460.3 eV, (c) for s-polarized, and (d) for p-polarized radiation.

photodoping (see Supplemental Material [19]). Even though there is a clear correlation between these states and oxygen treatment, quantification of the concentration of oxygen vacancies from the in-gap state intensity is problematic, as other potential sources and not only extrinsic defects can contribute to the intensity, as described in Ref. [25].

The experimental FS obtained with c-polarized photons for standard LAO/STO in Fig. 2(b) exhibits, intriguingly, nonequivalent shapes of the FS in different Brillouin zones, in agreement with Ref. [18]. This behavior comes from different matrix elements acting on the ARPES intensity from different interface bands, immediately revealing the multiband character of the LAO/STO interface states. The linear dichroism of the spectra, shown in Figs. 2(c) and 2(d), allows orbital decomposition of the experimental FS. Indeed, the FS should include a circle, originating mainly from Ti $3d_{xy}$ bands, and two ellipsoids, aligned along the k_x and k_y directions due to the heavy d_{yz} and d_{xz} band. Figure 2(c) clearly shows the cigar-shaped d_{yz} FS sheet elongated along the k_x axis, superimposed on the circular-shaped d_{xy} sheet. In Fig. 2(d), only the d_{xz} is visible as stretching along k_y. The matrix elements, modulating the intensity of each band, depend thus on the orbital character and experimental geometry, including the emission angle. Now we turn to the experimental band dispersions. Figures 3 and 4 show s-polarized and p-polarized ARPES data, respectively, along the Γ-X-Γ' direction, for both SD and LD samples. By switching between the p and s polarization, symmetric and antisymmetric states, respectively, relative to the (010) mirror plane (coinciding with the MP) should be excited. Indeed, entirely different dispersions are seen in the intensity plots [Figs. 3(a) and 3(e)] and, even more clearly, in the negative second-derivative plots ($-d^2I/dE^2 > 0$ only) of Figs. 3(b), 3(f), 4(b), and 4(e). Thus, consistently with the above FS maps, s polarization excites only the d_{xy}- and d_{yz}-derived states with their odd symmetry with respect to the (010) mirror plane, and p-polarized light excites only the d_{xz}-derived states with their even symmetry. Furthermore, the difference in experimental dispersions between the LD and SD samples highlights the effect of doping on the filling of individual bands.

Although the experimental energy resolution at this photon energy precludes resolving each individual Ti $3d$ band, the

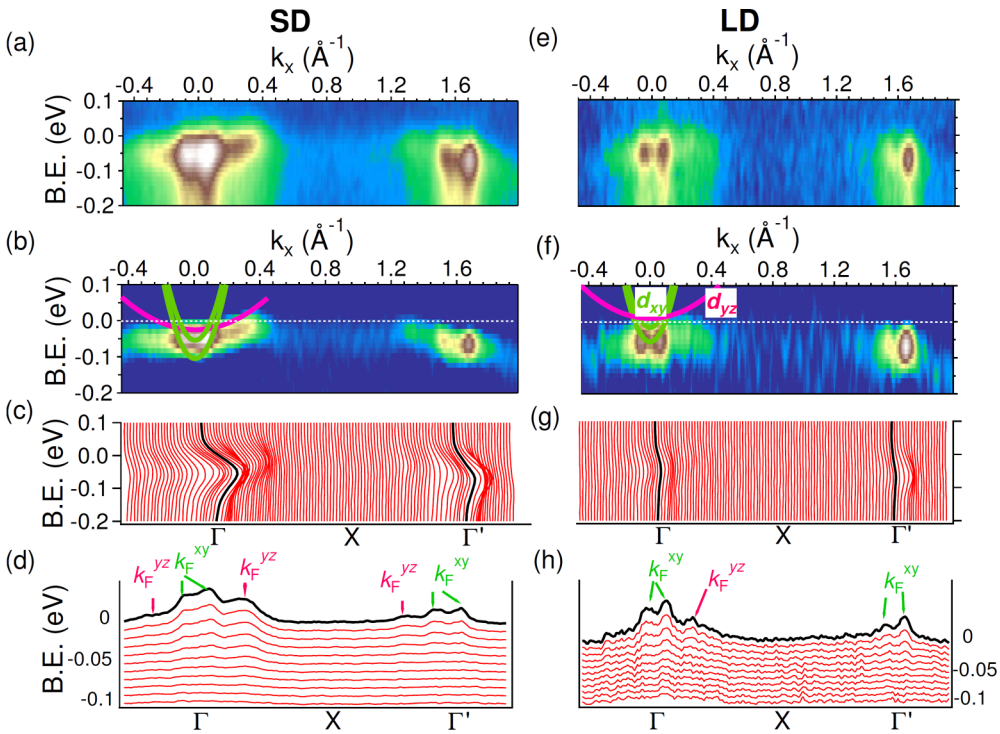

FIG. 3. (Color online) (a) ARPES data along the Γ-X-Γ' direction with s-polarized light and $h\nu = 460.3$ eV collected for a SD sample. (b) Second-derivative plot of data in (a) highlighting the band dispersion; (c) EDCs and (d) MDCs of the data in (a). (e)–(h) The equivalent measurements, but for a LD sample. (b),(f) The calculated t_{2g} parabolic bands. The color scale is the same as that in Fig. 2(b).

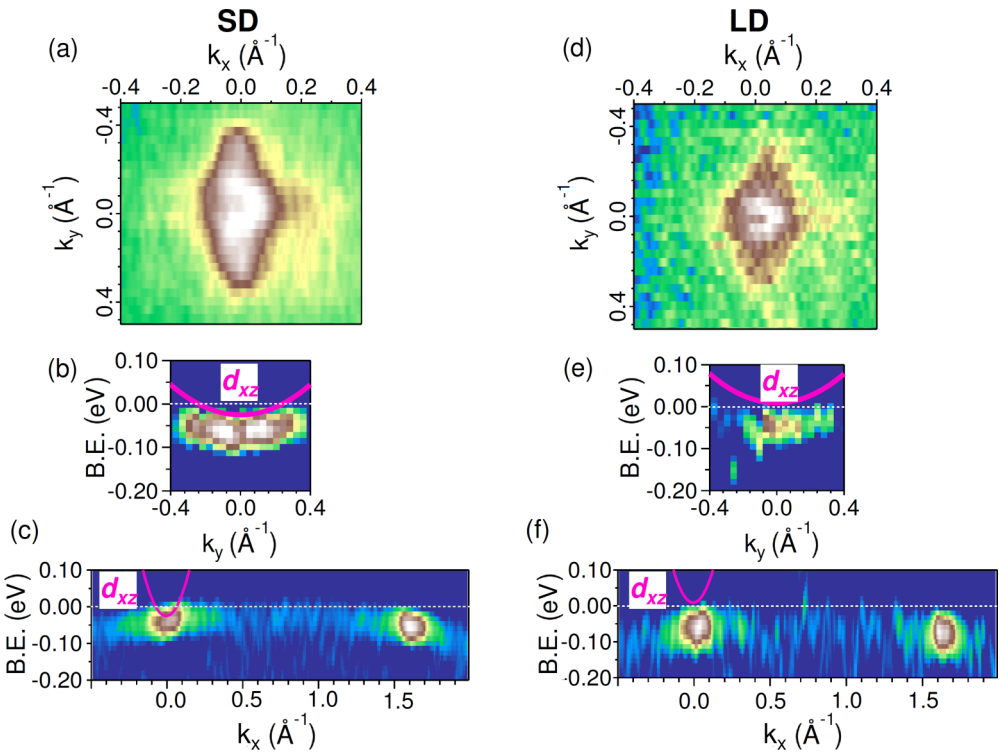

FIG. 4. (Color online) (a) FS collected with p-polarized light and $h\nu = 460.3$ eV. (b),(c) Second-derivative plots of ARPES data along the Γ-Y and Γ-X direction, respectively, for a SD sample with the calculated t_{2g} bands superimposed. (d)–(f) The equivalent measurements for a LD sample. The color scale is the same as in Fig. 2(b).

energy-distribution curves (EDCs) in Figs. 3(c) and 3(g) and the momentum distribution curves (MDCs) in Figs. 3(d) and 3(h) all show two types of bands, one lighter and one heavier (the latter having lower intensity in the second Brillouin zone). A comparison with the VPSIC-calculated t_{2g} bands for $Q = 0.04$ and 0.1, matching the experimental n_s values for LD and SD samples, respectively, superimposed on the ARPES data in Figs. 3(b) and 3(f), identifies the orbital character of these bands. At the SD sample carrier density, most of the charge is included in three bands. The lowest two bands have planar d_{xy} character, effective masses $m^* \approx 0.7$ along k_x, and Fermi vectors $k_F = 0.13$ Å^{-1} and 0.09 Å^{-1}. They represent the electronic charge entirely confined within the first and second TiO_2 layer from the interface (see the Supplemental Material [19]). The third occupied band has a d_{yz} character and includes charges spreading perpendicular to the interface. It is relatively flat along k_x ($m^* \approx 9$ and $k_F = 0.23$ Å^{-1}) and shifted upward in energy by about 70 meV with respect to the most occupied d_{xy} state. From the MDCs in Fig. 3(d), the different k_F associated with different bands are indicated; for the d_{xy} and d_{yz} orbitals, the experimental k_F values are 0.08 and 0.3 Å^{-1}, respectively, in good agreement with the calculated values. For the LD sample, the whole experimental band manifold shifts up, which qualitatively goes along with the decrease of n_s. The associated decrease of the Luttinger count of the FS surface is expressed by reduction of the d_{yz}-band k_F value to 0.17 Å^{-1}. This trend remains, however, on the qualitative level because the experimental d_{yz} band stays partly occupied (although strongly reduced in its spectral weight), whereas in the calculations, incorporating the experimental n_s, the d_{yz} band is entirely above E_F. We notice that the experimental bands, also for the SD sample, are systematically lower compared to the calculations, indicating more coherent carriers than in the transport measurements. This discrepancy can hardly be explained by a possible polaronic satellite of the d_{yz} band [28] because it would be broader in energy and separated from the main band above 100 meV, which is much larger than the observed shift of the d_{yz}. We conjecture that this deficiency may be caused by certain charge localization mechanisms [29] such as the Anderson localization beyond the mobility edge [30], deep-level trapping, or certain disordered phase separations.

The p-polarization results are shown in Fig. 4. By symmetry, only the d_{xz} bands are expected to appear, thus here we superimpose only the calculated d_{xz} band (the magenta lines in Fig. 4). Due to tetragonal symmetry, the d_{xz}-band bottom is degenerate with d_{yz}, and its effective mass along k_y is equal to that of d_{yz} along k_x. Thus, for the SD sample, ARPES displays a rather flat band enclosed in a cigar-shaped Fermi pocket of length $k_y \sim 0.3$ Å^{-1}, in good agreement with the value 0.23 Å^{-1} calculated for $n_s = 6.5 \times 10^{13}$ e/cm^2 [see Figs. 4(b) and 4(c)]. On the other hand, assuming again $n_s = 2.6 \times 10^{13}$ e/cm^2 for the calculation of the LD sample, the d_{xz} band lies entirely above E_F [see Figs. 4(e) and 4(f)]. Shrinking of the orbital occupancy in the LD sample is also seen in the FS map in Fig. 4(d), in comparison with Fig. 4(a), and in the second-derivative plots in Figs. 4(e) and 4(f). Although there is some remnant d_{xy} signal (due to the finite acceptance of the analyzer and possible defect scattering on the LAO overlayer), importantly, the d_{xz}-band occupancy is lower at lower charge concentrations. For both SD and LD

samples, consistently with data collected for s-polarized light, a similar shift between the measured and calculated bands is observed.

We note that for all samples, the dispersion range of the bands is limited to less than 0.1 eV below E_F. This value is significantly smaller than the 0.4 eV reported in Ref. [18], the latter possibly reflecting the incoherent weight below the main spectral function peak, due to the lower energy resolution. From our experimental observations, it is clear how the ideal limit dictated by the polar catastrophe ($n_s = 3.3 \times 10^{14}$ e/cm^2, corresponding to half an electron per interface u.c.) is not achieved in actual samples. The theoretical band bottom energies, indeed, at this high electron density are located at -370, -210, and -100 meV for the d_{xy} (Ti_1), d_{xy} (Ti_2), and d_{xz}-band bottoms, respectively [6], clearly incompatible with the ARPES data.

The experimental polarization-dependent ARPES data qualitatively demonstrate the evolution of electronic structure going along the change in carrier concentration between the LD and SD samples. These results differ from the ARPES measurements on bare STO despite the qualitative similarities in the shape. In contrast to the universal 2D FS of bare STO, whose size and shape are decoupled from the bulk-sample preparation, it appears that the deposition conditions of LAO affect the LAO/STO 2D FS size.

In conclusion, we have performed polarization-dependent ARPES, investigating the symmetry of the valence states and band structure of LAO/STO interfaces for different dopant concentrations. The d_{xy}, $d_{yz,xz}$ bands are clearly distinguished and can be compared to those from *ab initio* calculations. From first-principles calculations, we have shown that the position of the $3d$ levels strongly depends on the mobile and localized charge. For both samples, ARPES spectra are qualitatively consistent with the electronic band structures calculated for doping concentrations fixed to the values obtained from Hall measurements, but deviate from the band structure calculated for the ideal limit of 0.5 e/u.c. expected from the polar catastrophe scenario. This demonstrates that Hall measurements can be correlated to the occupancy of the delocalized $3d$ levels at the interface. This work thus provides benchmark results linking the evolution of the band structure to the sheet carrier density.

The authors are grateful to J.-M. Triscone, S. Gariglio, D. Stornaiuolo, and A. Fête for discussion and help in sample preparation. The Schweizerischer Nationalfonds zur Förderung der wissenschaftlichen Forschung, in particular the National Center of Competence in Research, Materials with Novel Electronic Properties (MaNEP), is gratefully acknowledged. CNR-IOM scientists acknowledge MIUR-PRIN 2010 *Oxide*, IIT-Seed NEWDFESCM, IIT-SEED POLYPHEMO, and "platform computation" of IIT, and Fondazione Banco di Sardegna grants. Ph.G. acknowledges support from a Research Professorship of the Francqui Foundation and partial financial support from the ARC project TheMoTherm.

[1] A. Ohtomo and H. Y. Hwang, Nature (London) **427**, 423 (2004).

[2] N. Reyren, S. Thiel, A. D. Caviglia, L. Fitting Kourkoutis, G. Hammerl, C. Richter, C. W. Schneider, T. Kopp, A.-S. Rüetschi, D. Jaccard, M. Gabay, D. A. Muller, J.-M. Triscone, and J. Mannhart, Science **317**, 1196 (2007).

[3] A. D. Caviglia, S. Gariglio, N. Reyren, D. Jaccard, T. Schneider, M. Gabay, S. Thiel, G. Hammerl, J. Mannhart, and J.-M. Triscone, Nature (London) **456**, 624 (2008).

[4] S. Thiel, G. Hammerl, A. Schmehl, C. W. Schneider, and J. Mannhart, Science **313**, 1942 (2006).

[5] Z. S. Popovic, S. Satpathy, and R. M. Martin, Phys. Rev. Lett. **101**, 256801 (2008).

[6] P. Delugas, A. Filippetti, V. Fiorentini, D. I. Bilc, D. Fontaine, and P. Ghosez, Phys. Rev. Lett. **106**, 166807 (2011).

[7] N. Nakagawa, H. Y. Hwang, and D. A. Muller, Nat. Mater. **5**, 204 (2006).

[8] S. Gariglio, N. Reyren, A. D. Caviglia, and J.-M. Triscone, J. Phys.: Condens. Matter **21**, 164213 (2009).

[9] Y. Xie, Y. Hikita, C. Bell, and H. Y. Hwang, Nat. Commun. **2**, 494 (2011).

[10] N. C. Bristowe, P. B. Littlewood, and E. Artacho, Phys. Rev. B **83**, 205405 (2011).

[11] W. Meevasana, P. D. C. King, R. H. He, S.-K. Mo, M. Hashimoto, A. Tamai, P. Songsiriritthigul, F. Baumberger, and Z.-X. Shen, Nat. Mater. **10**, 114 (2011).

[12] A. F. Santander-Syro, O. Copie, T. Kondo, F. Fortuna, S. Pailhes, R. Weht, X. G. Qiu, F. Bertran, A. Nicolaou, A. Taleb-Ibrahimi, P. Le Fevre, G. Herranz, M. Bibes, N. Reyren, Y. Apertet, P. Lecoeur, A. Barthelemy, and M. J. Rozenberg, Nature (London) **469**, 189 (2011).

[13] N. C. Plumb, M. Salluzzo, E. Razzoli, M. Månsson, M. Falub, J. Krempasky, C. E. Matt, J. Chang, M. Schulte, J. Braun, H. Ebert, J. Minár, B. Delley, K.-J. Zhou, T. Schmitt, M. Shi, J. Mesot, L. Patthey, and M. Radović, arXiv:1302.0708.

[14] M. Kobayashi, I. Muneta, T. Schmitt, L. Patthey, S. Ohya, M. Tanaka, M. Oshima, and V. N. Strocov, Appl. Phys. Lett. **101**, 242103 (2012).

[15] G. Drera, F. Banfi, F. F. Canova, P. Borghetti, L. Sangaletti, F. Bondino, E. Magnano, J. Huijben, M. Huijben, G. Rijnders, and D. H. A. Blank, Appl. Phys. Lett. **98**, 052907 (2011).

[16] A. Koitzsch, J. Ocker, M. Knupfer, M. C. Dekker, K. Dörr, B. Büchner, and P. Hoffmann, Phys. Rev. B **84**, 245121 (2011).

[17] C. Cancellieri, M. L. Reinle-Schmitt, M. Kobayashi, V. N. Strocov, T. Schmitt, P. R. Willmott, S. Gariglio, and J.-M. Triscone, Phys. Rev. Lett. **110**, 137601 (2013).

[18] G. Berner, M. Sing, H. Fujiwara, A. Yasui, Y. Saitoh, A. Yamasaki, Y. Nishitani, A. Sekiyama, N. Pavlenko, T. Kopp, C. Richter, J. Mannhart, S. Suga, and R. Claessen, Phys. Rev. Lett. **110**, 247601 (2013).

[19] See Supplemental Material at http://link.aps.org/supplemental/10.1103/PhysRevB.89.121412 for photoemission on related $La_{0.5}Sr_{0.5}Al_{0.5}Ti_{0.5}O_3$/STO heterostructures, resonant photoemission spectroscopy and x ray absorption spectroscopy maps, photodoping, magnetotransport measurements, and details on *ab initio* calculations for electronic bands at different Q values.

[20] C. Cancellieri, N. Reyren, S. Gariglio, A. D. Caviglia, A. Fête, and J.-M. Triscone, Europhys. Lett. **91**, 17004 (2010).

[21] A. D. Caviglia, M. Gabay, S. Gariglio, N. Reyren, C. Cancellieri, and J.-M. Triscone, Phys. Rev. Lett. **104**, 126803 (2010).

[22] A. Filippetti, C. D. Pemmaraju, S. Sanvito, P. Delugas, D. Puggioni, and V. Fiorentini, Phys. Rev. B **84**, 195127 (2011).

[23] V. N. Strocov, T. Schmitt, U. Flechsig, T. Schmidt, A. Imhof, Q. Chen, J. Raabe, R. Betemps, D. Zimoch, J. Krempasky, X. Wang, M. Grioni, A. Piazzalunga, and L. Patthey, J. Synchrotron Radiat. **17**, 631 (2010).

[24] M. L. Reinle-Schmitt, C. Cancellieri, D. Li, D. Fontaine, M. Medarde, E. Pomjakushina, C. W. Schneider, S. Gariglio, P. Ghosez, J.-M. Triscone, and P. R. Willmott, Nat. Commun. **3**, 932 (2012).

[25] Y. Ishida, R. Eguchi, M. Matsunami, K. Horiba, M. Taguchi, A. Chainani, Y. Senba, H. Ohashi, H. Ohta, and S. Shin, Phys. Rev. Lett. **100**, 056401 (2008).

[26] N. C. Plumb, M. Kobayashi, M. Salluzzo, E. Razzoli, C. Matt, V. N. Strocov, K.-J. Zhou, C. Monney, T. Schmitt, M. Shi, J. Mesot, L. Patthey, and M. Radović, arXiv:1304.5948.

[27] Y. Aiura, I. Hase, H. Bando, T. Yasue, T. Saitoh, and D. Dessau, Surf. Sci. **515**, 61 (2002).

[28] Y. J. Chang, A. Bostwick, Y. S. Kim, K. Horn, and E. Rotenberg, Phys. Rev. B **81**, 235109 (2010).

[29] K.-J. Zhou, M. Radovic, J. Schlappa, V. Strocov, R. Frison, J. Mesot, L. Patthey, and T. Schmitt, Phys. Rev. B **83**, 201402 (2011).

[30] D. C. Licciardello and D. J. Thouless, J. Phys. C: Solid State Phys. **8**, 4157 (1975).